Chapter 2
The Large Hadron Collider and the CMS Experiment

Abstract This chapter is dedicated to the description of the experimental apparatus which made these measurements possible. Section 2.1 describes the Large Hadron Collider, the accelerator which provided 7 TeV proton-proton collisions which were analysed in this thesis. The collisions were reconstructed with the Compact Muon Solenoid (CMS) detector, to which Sect. 2.2 is dedicated to. The two final sections of this chapter illustrate the lepton reconstruction techniques adopted in CMS.

2.1 The Large Hadron Collider

The Large Hadron Collider (LHC) at CERN is the largest and most energetic particle accelerator ever built. It occupies the 27 km long tunnel previously hosting the LEP collider, about 100 m underneath the surface across the French-Swiss national border near Geneva. It is a superconducting proton-proton collider, capable of producing collisions at a center of mass energy of up to 14 TeV, and a maximal instantaneous luminosity of 10^{34} cm^{-2} s^{-1}. It has been delivering 7 TeV proton collisions since March 2010, and it is expected to raise its center of mass energy in the coming years.

The LHC proton injection chain is schematically shown in Fig. 2.1. Protons are accelerated three times before they enter the LHC ring: the LINAC brings them to 50 MeV, the Proton Synchrotron (PS) to 1.4 GeV, and finally the Super Proton Synchrotron (SPS) injects them into the LHC at 450 GeV. The LHC then completes the acceleration by bringing them to 7 TeV with its 400 MHz radiofrequency cavities, capable of 'kicks' which result in increases of the proton energy of 0.5 MeV per turn.[1]

Since the collisions occur between particles of the same electrical charge, two separate acceleration cavities and two different magnetic field configurations are required. The LHC is equipped with 1232 superconducting 14.2 m long Niobium-Titanium dipole magnets, cooled down to 1.9 K by means of super-fluid Helium, that

[1] The LHC is also capable of accelerating and colliding beams of lead ions at 2.76 TeV in the center of mass per nucleon. As this is not relevant for this thesis, it will not be treated.

F. Pandolfi, *Search for the Standard Model Higgs Boson in the $H \to ZZ \to \ell^+\ell^- q\bar{q}$ Decay Channel at CMS*, Springer Theses, DOI: 10.1007/978-3-319-00903-2_2,

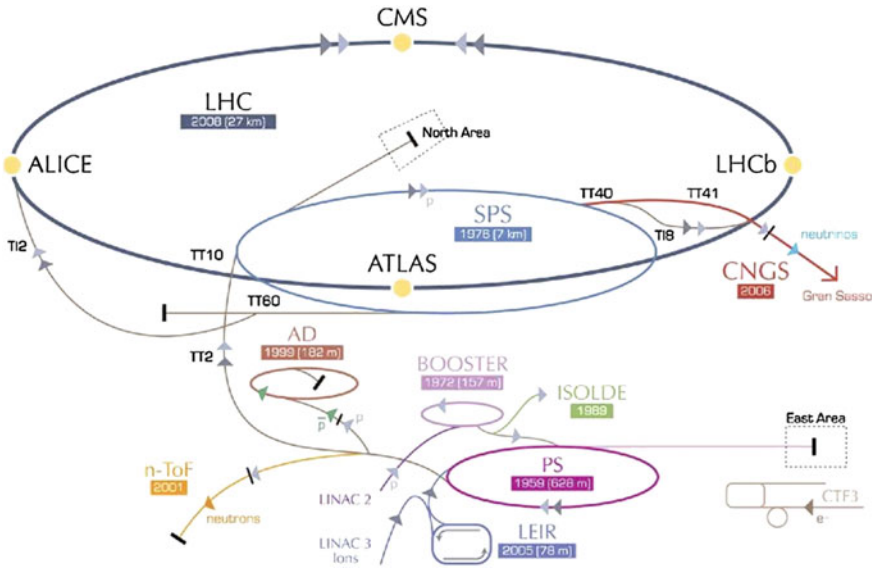

Fig. 2.1 Schematic view of the LHC injection scheme

create a bending magnetic field of about 8.3 T. The magnets are placed in the eight curved sections which connect the straight sections of the LHC ring.

The high luminosity of the LHC is obtained by a high frequency bunch crossing and a high number of protons per bunch: two beams of protons with an energy of up to 7 TeV (3.5 TeV in the initial physics runs), circulating in two different vacuum chambers, contain each up to 2,808 bunches. The bunches, with a nominal number of 10^{11} protons each, have a very small transverse spread (about 15 μm in the transverse directions) and are about 7.5 cm long in the beam direction at the interaction points. The bunches cross at the rate of up to 40 MHz, i.e. one collision each 25 ns. A summary of the principal LHC technical parameters is given in Table 2.1.

The LHC can cross its beams in four interaction points. Two of them have high luminosity and are dedicated to the general purpose experiments ATLAS [1] and CMS. The other two, at lower luminosity, serve the ALICE [2] and LHCb [3] experiments, respectively focused on heavy ion physics and CP violation measurements.

The operating conditions at the LHC are extremely challenging for the experiments. The total proton-proton cross section is estimated to be about 100 mb [4], which implies about 20 proton interactions per bunch crossing, i.e. 10^9 interactions per second. A strong online event selection is therefore required in order to reduce the event rate at $\mathcal{O}$ (100) Hz, corresponding to the maximum data storage rate sustainable by the existing device technology. The detectors must also have a fast response time (around 25 ns) and a fine granularity in order to minimize the performance degradation in simultaneous events. In addition to this, the high flux of particles coming from proton interactions implies that each component of the detector has to be radiation

Table 2.1 Summary of the principal LHC technical parameters

Circumference [km]	27
Number of magnet dipoles	1,232
Dipolar magnetic field [T]	8.33
Radiofrequency [MHz]	400
Maximal number of bunches	2,808
Magnet temperature [K]	1.9
Maximal beam energy [TeV]	7
Maximal luminosity [$cm^{-2}s^{-1}$]	10^{34}
Initial beam energy [TeV]	3.5
Protons per bunch	$1.05 \cdot 10^{11}$
Bunch spacing [m]	7.48
Minimal bunch time separation [ns]	25
Bunch length [cm]	7.5
Bunch transverse size [μm]	15
Crossing angle [rad]	$2 \cdot 10^{-4}$
Beam lifetime [h]	7
Luminosity lifetime [h]	10

resistant. Finally, to fully understand the physical processes occurring at the LHC, multi-purpose detectors are required to satisfy the following requirements:

- full hermeticity, in order to provide accurate measurements of missing transverse energy;
- excellent reconstruction of high-energy leptons and photons;
- precise determination of charged particle momenta and impact points through an efficient tracking system;
- accurate reconstruction of hadronic activity from QCD processes and heavy particle decays.

The Compact Muon Solenoid detector meets all these stringent requirements. It is described in the following.

2.2 The CMS Experiment

The Compact Muon Solenoid (CMS) experiment [5] is one of the two general-purpose detectors which take data at the LHC. One of the cardinal points of its scientifical program is the discovery of the Higgs boson. Its design philosophy has therefore been driven by such a search, and can be summarized by the following points:

- an excellent and redundant muon system. This has lead to the choice of a large, superconducting solenoidal magnet, capable of producing a 4 T field, which allows to have a compact muon spectrometer, delivering precise track and unambiguous charge measurements for muons of transverse momenta up to 1 TeV;

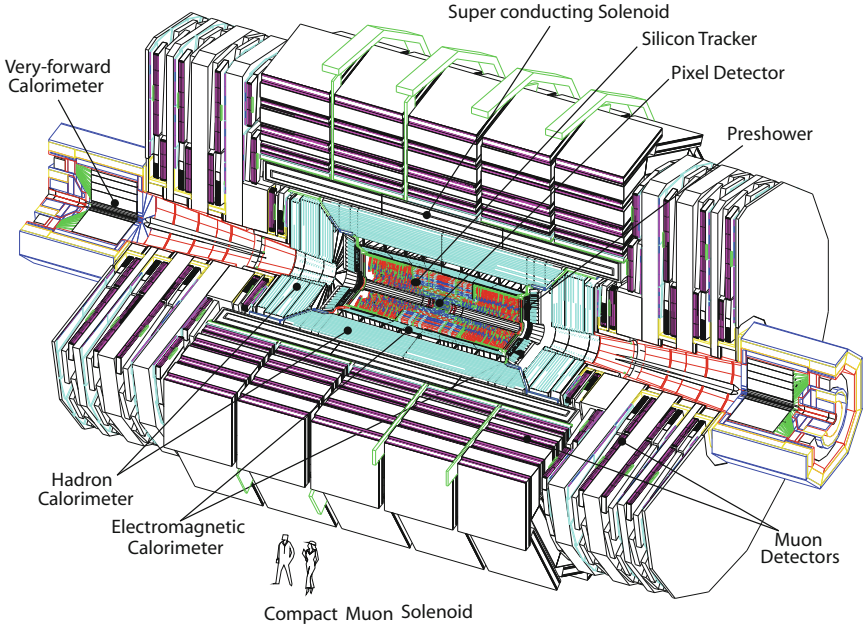

Fig. 2.2 An exploded view of the CMS detector

- the best possible electromagnetic calorimeter compatible with the magnet;
- a precise and efficient inner tracking system;
- a highly hermetic hadronic calorimeter system, capable of delivering good performance in missing transverse energy reconstruction.

The structure of the CMS detector is shown in Fig. 2.2. It has a cilindrical shape, symmetrical around the beam direction, with a radius of 7.5 m, a total length of 22 m, and weighs about 12, 500 tons. It is divided into a central section, made of several layers coaxial to the beam axis (the *barrel*), closed at its ends by two hermetic discs orthogonal to the beam (the *endcaps*).

A schematic view of a transverse section of CMS is visible in Fig. 2.3. Moving outwards starting from the beam position, it presents a silicon tracker, a crystal electromagnetic calorimeter, a hadronic calorimeter, and the superconducting solenoidal magnet, in the return yoke of which the muon drift chambers are inserted.

The coordinate system adopted in CMS is cartesian, has the origin centered in the nominal collision point at the center of the detector, and adopts the following conventions:

- the x axis points towards the center of the LHC ring;
- the z direction coincides with the CMS cylinder axis;
- the y axis points upwards, towards the surface.

The cylindrical symmetry of the apparatus drives the use of a pseudo-angular reference system, given by the triplet of variables (r,ϕ,η), where r is the radial distance

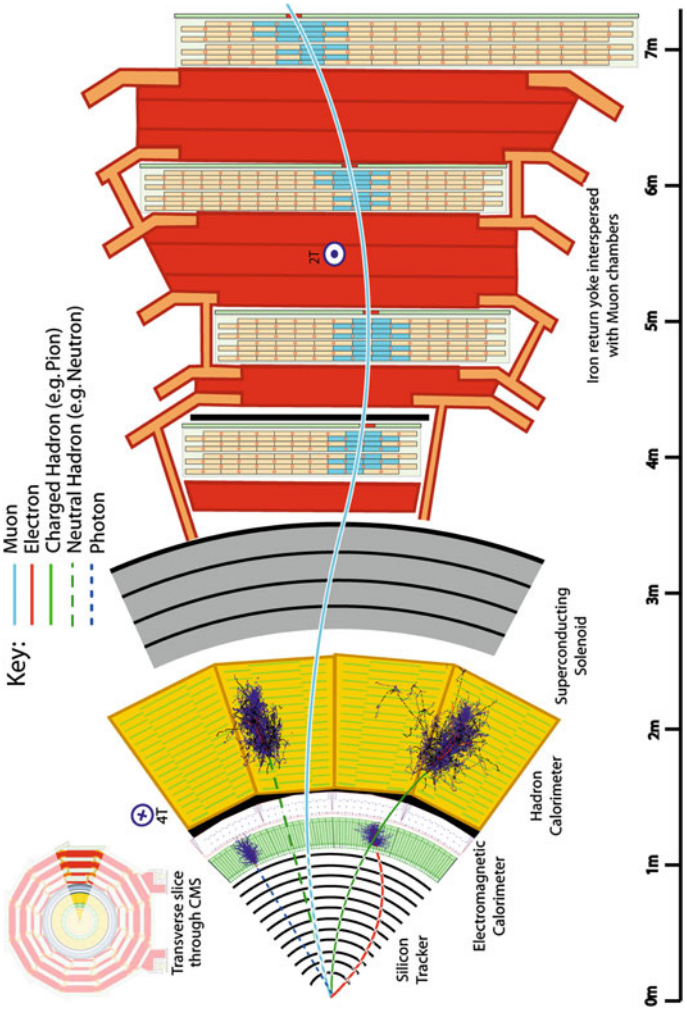

Fig. 2.3 Schematic view of a transverse slice of the central part of the CMS detector

from the beam axis, ϕ is the aximuthal angle with respect to the x axis, and η, commonly referred to as *pseudorapidity*, is defined as

$$\eta = -\ln \tan \frac{\theta}{2}$$

where θ is the polar angle with respect to the z axis. The use of the pseudorapidity is motivated by the fact that for high energies it is a good approximation of the rapidity (y) of a particle, defined as

$$y = \frac{1}{2} \ln \left(\frac{E + p_{\mathrm{L}}}{E - p_{\mathrm{L}}} \right)$$

where E is the particle's energy and p_{L} is the component of its momentum projected along the beam axis. The rapidity is a useful variable at a hadron collider, as it is invariant, expect for a constant additive term, under Lorentzian boosts along the axis direction. It follows from its definition that the pseudorapidity is null for $\theta = 0$ and increases in absolute value when approaching the beam pipe, asymptotically reaching infinity at $\theta = \pi/2$ (on the z axis).

We furthermore denote with p_{T} the component of a particle's momentum in the plane transverse to the beam axis, and with E_{T} its transverse energy, obtained from its energy by $E_{\mathrm{T}} = E \cdot \sin \theta$.

We will now provide a brief description of the subdetectors which constitute CMS.

2.2.1 Magnet

In order to achieve a compact and high-resolution muon detection system, a large bending power is required. This can be achieved by a relatively small solenoid, provided that an intense magnetic field is produced, as the bending starts at the collision vertex. A large enough length/radius ratio is also demanded for, in order to ensure good momentum resolution in the forward region as well.

These considerations led to the choice [6] of a 13 m long superconducting cylindrical Niobium-Titanium coil, with a diameter of 5.9 m. It provides a uniform magnetic field of 3.8 T at its center, carrying a current of 18 kA and a total stored magnetic energy of 2.4 GJ. The magnet flux is returned by a saturated iron yoke, which also works as mechanical support structure of the detector.

2.2.2 Tracker

The design goal of the inner tracking system is to reconstruct isolated, high-p_{T} electrons and muons with efficiency greater than 95 %, and tracks of particles within jets with efficiency greater than 90 %, within a pseudorapidity coverage of $|\eta| < 2.4$. At the same time it must comply to severe material budget constraints, in order not to

Table 2.2 Expected radiation dose and charged particle flux at different radii in the barrel of the CMS tracker, for the high-luminosity run of the LHC and an integrated luminosity of 500 fb^{-1}

Radius (cm)	Radiation dose (kGy)	Charged particle flux ($\text{cm}^{-2}\text{s}^{-1}$)
4	840	10^8
22	70	$6 \cdot 10^6$
115	1.8	$3 \cdot 10^5$

degrade its momentum resolution. All of this must be achieved in a high-multiplicity, highly radioactive environment such as the one created by LHC collisions.

This led to the choice of a large silicon tracker [7]. It is the first example in high-energy physics of an inner tracking system completely based on this technology alone. Referring to Table 2.2, which summarizes the expected dose of radiation and charged particle flux for the high-luminosity run of the LHC, we can identify three tracker regions:

- closest to the interaction vertex where the particle flux is highest ($\approx 10^7$/s at $r \approx 10$ cm), pixel detectors are placed. The size of a pixel is about 100×150 μm^2, giving an occupancy of about 10^{-4} per pixel per high-luminosity LHC crossing;
- the intermediate region ($20 < r < 55$ cm), where the particle flux is low enough to enable the use of silicon microstrip detectors with a minimum cell size of 10 cm $\times$ 80 μm, leading to an occupancy of $\approx$ 2–3 %/crossing;
- the outermost region ($r > 55$ cm) of the inner tracker, where the particle flux has dropped sufficiently to allow the adoption of larger-pitch silicon microstrips with a maximum cell size of 25 cm $\times$ 180 μm, whilst keeping occupancy around 1 %.

Even in heavy-ion (Pb-Pb) running, the occupancy is at the level of 1% in the pixel detectors and less than 20 % in the outer silicon strip detectors, permitting track reconstruction in such a high density environment.

The layout of the pixel detector is shown in Fig. 2.4: it features three cylindrical layers in the barrel region, placed respectively at radii of 4.7, 7.3 and 10.2 cm, and

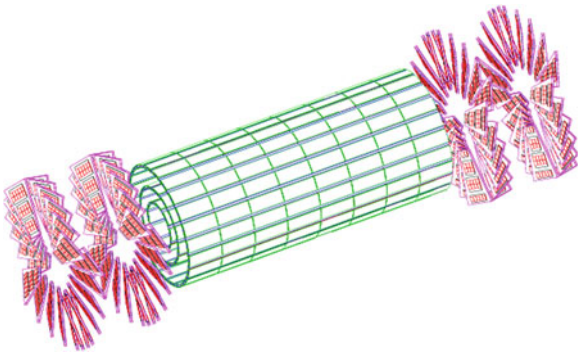

Fig. 2.4 Layout of the CMS silicon pixel detector

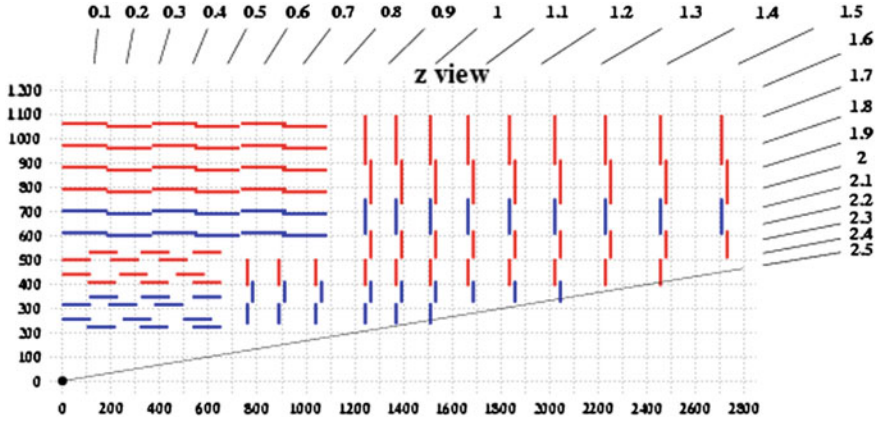

Fig. 2.5 Schematic longitudinal section of one quarter the CMS silicon microstrip detector. The nominal interaction point is in the *bottom-left corner*. Distances are marked in *millimeters on the left and bottom axes*, and pseudorapidity values are shown on the *top and right borders*

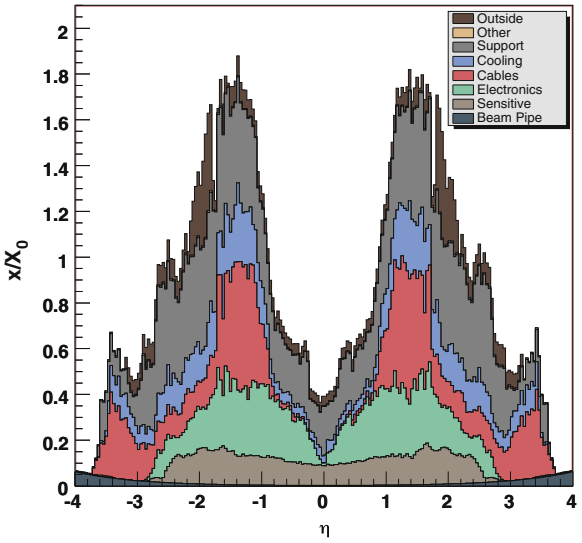

Fig. 2.6 Silicon tracker material budget as a function of pseudorapidity, expressed in units of radiation lengths (X_0). Different material categories are shown: beam pipe, silicon sensitive volumes, electronics, cables, cooling pipes and fluid, support mechanics and outer structures

two closing end-discs, extending from 6 to 15 cm in radius, and placed on each side at $|z| = 34.5$ cm and 46.5 cm. This design ensures that each charged particle produced within $|\eta| = 2.2$ releases at least two hits in the pixel detector.

The pixel layers are enveloped by a silicon microstrip detector, a section of which is schematically represented in Fig.2.5. The barrel microstrip detector is divided in

two regions: the inner and outer barrel. The inner barrel is made of four layers (the two innermost of which are double-sided), and cover the depth $20 < r < 55$ cm. The outer barrel counts six layers (the two innermost double-sided) and reach up to a radius of 110 cm. In order to avoid that particles hit the sensitive area at too small angles, the inner barrel is shorter than the outer region, and three additional disc-shaped layers have been inserted, between the inner barrel and the endcaps. The endcap detector is made of nine layers of discs, up to a maximum distance of $z = 270$ cm. The first, second, and fifth layers are double-sided.

The silicon tracker detector comprises of a total of 66 million pixel and 9.6 million strip channels. Its material budget in units of interaction lengths, as a function of pseudorapidity, is shown in Fig. 2.6. As can be seen, it adds up to less than half a radiation length in the center of the barrel, increasing to a maximum of about 1.8 X_0 in the barrel-endcap transition ($|\eta| \sim 1.5$).

2.2.3 Electromagnetic Calorimeter

A high-performance electromagnetic calorimeter is a cardinal element of a general purpose high-energy physics detector, as it allows precise measurements of photon and electron energies. The CMS collaboration has opted [8] for a hermetic, homogeneous electromagnetic calorimeter (ECAL), made of 61 200 lead tungstate ($PbWO_4$) scintillating crystals mounted in the barrel region, and closed by two endcaps, which count 7 324 crystals each.

The main characteristics of $PbWO_4$ are listed in Table 2.3. The choice of this inorganic crystal has been determined by a number of factors:

- its short radiation length (0.89 cm) allows the construction of a compact calorimeter, which can comply to the requirements imposed by the magnet radius;
- its small Molière radius (2.2 cm) ensures an efficient lateral shower containment, and therefore high granularity;
- it is characterized by a very fast light emission process (its principal and secondary scintillation components have emission times respectively of 5 and 15 ns), a crucial feature at a collider where bunch crossings are interspaced by only 25 ns;

Table 2.3 Main characteristics of lead tungstate ($PbWO_4$) The superscripts f and s respectively denote the principal (*fast*) and secondary (*slow*) scintillation emissions

Radiation length (cm)	0.89
Density (g cm^{-3})	8.3
Molière radius (cm)	2.2
Refractive index	2.29
Light Yield (γ/MeV)	30
Light emission time (ns)	5^f
	15^s
Scintillation wavelength (nm)	440^f
	480^s

- it is sufficiently radiation hard, allowing it to sustain several years of high-luminosity running with tolerable degradation of the crystals transparency, which can be corrected with a light monitoring system.

However, the relatively low light yield (30 γ/MeV) necessitates the use of photodetectors with high intrinsic gain and which can operate in a magnetic field. This led to the use of silicon avalanche photodiodes (APD) in the barrel, and vacuum phototriodes (VPT) in the endcaps.

A longitudinal section of a quarter of the ECAL is shown in Fig. 2.7. The barrel covers the pseudorapidity region $|\eta| < 1.479$ and has an inner radius of 129 cm. It is made of 18 identical supermodules, each of which covers half the barrel length. It has a granularity of 360 crystals in the azimuthal direction (ϕ), and (2×85) crystals in η. The crystals are organized in a quasi-projective geometry, so that their axes form a 3° angle with the line that connects them to the nominal interaction point. A single crystal corresponds to a 0.0174×0.0174 square in the $\eta - \phi$ plane, and its front face measures about 22×22 mm^2. They are 23 cm long, equivalent to 25.8 X_0.

The endcaps are placed at a distance of 3.144 m from the nominal interaction point and reach up to $|\eta| = 3$. They are made of identical crystals, with a front face of 28.62×28.62 mm^2 and a length of 22.0 cm (24.7 X_0). They are grouped in 5×5 mechanical units, called *supercrystals*.

The front face of the endcaps is equipped, in the $1.653 < |\eta| < 2.6$ pseudorapidity interval, with a preshower detector. It is a two-layer sampling calorimeter, which uses lead as absorber and silicon strips as active material. The thickness of the two lead absorbers is respectively 2 X_0 and 1 X_0.

The energy resolution of a homogeneous calorimeter may be parametrized with the following expression:

$$\frac{\sigma}{E} = \frac{S}{\sqrt{E}} \oplus \frac{N}{E} \oplus C$$

The stochastic (S), noise (N), and constant (C) terms of the ECAL have been measured at a test beam [9], and were found to have a value of:

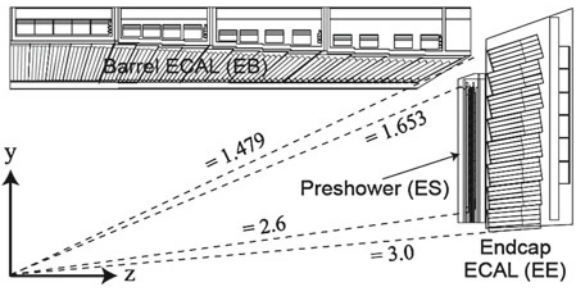

Fig. 2.7 Longitudinal section of a quarter of ECAL

$$S = 2.8\%\ \text{GeV}^{1/2} \qquad N = 124\ \text{MeV} \qquad C = 0.3\,\%$$

2.2.4 Hadronic Calorimeter

The role of the hadronic calorimeter [10] is to contain the showers of hadronic particles, and therefore measure jet quadrimomenta and the missing transverse energy of events. The two key features for these tasks are a high hermeticity and a good transverse granularity. Furthermore, a good energy resolution and a sufficient longitudinal containment are also important.

A longitudinal section of a quarter of the hadronic calorimeter is shown in Fig. 2.8. It is formed by two separate detectors: a central (HCAL) and a forward (HF) calorimeter. The HCAL covers the pseudorapidity range $|\eta| < 3$, and is in turn divided into two subdetectors: a barrel ($|\eta| < 1.3$) and two endcaps ($1.3 < |\eta| < 3$). It is a sampling calorimeter, with brass used as absorber and plastic scintillators as active material. It has a transverse granularity of $\Delta\eta \times \Delta\phi = 0.087 \times 0.087$.

The energy resolution of the HCAL is parametrized as

$$\frac{\sigma}{E} = \frac{100\,\%}{\sqrt{E\,(\text{GeV})}} \oplus 8\,\%$$

for pions of energy E. It has a total thickness of 7–10 interaction lengths (λ_i). A depth of $7\lambda_i$ is not sufficient to ensure the complete containment of a highly energetic hadronic shower, therefore an additional layer of active material was added behind the solenoid, which increases the total effective thickness by about $3\lambda_i$ and improves by 10 % the energy resolution for 300 GeV pions.

To improve the detector's hermeticity, an additional calorimeter (HF) is placed outside the magnet yoke, 11 m away from the interaction point, on both sides. It covers the very forward pseudorapidity region $3 < |\eta| < 5$. In order to sustain the very

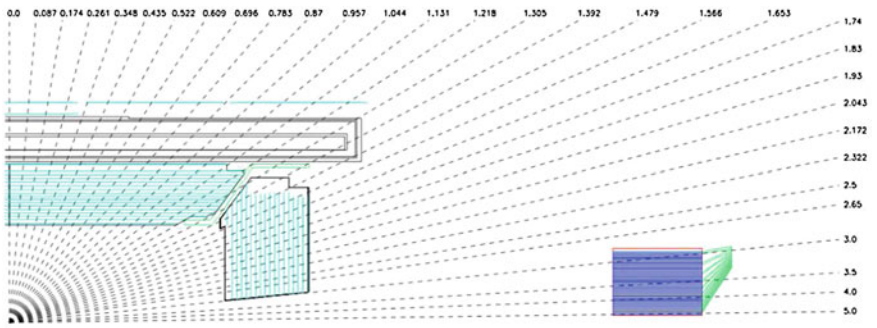

Fig. 2.8 Longitudinal section of a quarter of the CMS hadronic calorimeters: HCAL is visible on the *left*, HF far away from the interaction point on the *right*. Some values of pseudorapidity are marked

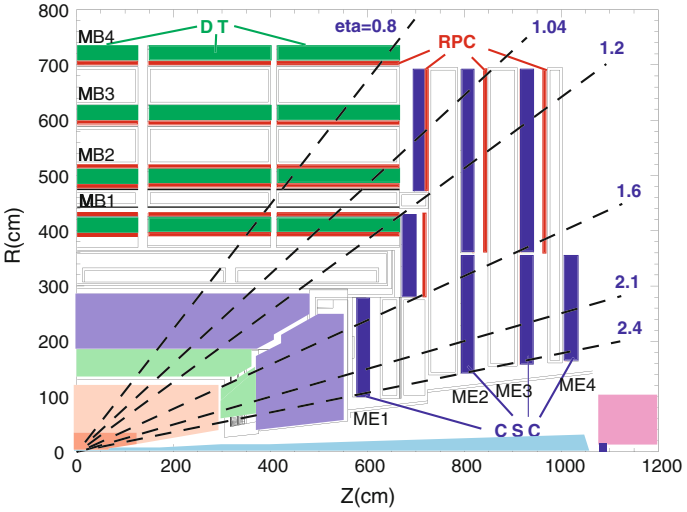

Fig. 2.9 Longitudinal section of a quarter of the CMS muon system

high doses of radiation and high particle multiplicities expected for such a region, they are sampling calorimeters made of iron and quartz fibers. The fibers are of two different lengths, the longer ones reach the front face of the calorimeter, the short ones end 22 cm before that. In this way, most of the electromagnetic component of the hadronic showers will be released in the long fibers, and can therefore be isolated by subtraction. Its granularity is $\Delta\eta \times \Delta\phi = 0.175 \times 0.175$.

2.2.5 Muon System

The muon system [11] has the aim of detecting muons, the only charged particles which are able to pass through the calorimeters without being absorbed. It is placed outside the magnet coil, and it has a pseudorapidity reach of $|\eta| < 2.4$. It is subdivided in a barrel and two endcaps, and the two regions use different technologies. Both regions are made of four layers of measuring stations, imbedded in the iron of the magnet return yoke, where the return field of the solenoid is about 1.5 T. A schematic longitudinal section of a quarter of the CMS muon system is shown in Fig. 2.9.

The barrel region ($|\eta| < 1.2$) is made of drift tube (DT) stations, each of which is made of 12 planes of tubes, for a total of 195, 000 tubes. The endcaps ($1.2 < |\eta| < 2.4$) have to cope with an intense magnetic field and a higher particle multiplicity, therefore cathode strip chamber (CSC) detectors are employed, organized in six-layer modules. CSC's are multi-wire proportional chambers in which the cathode plane has been segmented into strips.

In addition to this, both barrel and endcaps are equipped with resistive plate chamber (RPC) detectors, which are parallel-plate gas chambers with an excellent (3 ns)

time resolution. The RPC's supply a very fast trigger system, capable of identifying muons with high efficiency. They are organized in six barrel and four endcap stations, for a total of 612 chambers.

2.2.6 Trigger

At the nominal LHC luminosity the event rate is expected to reach 10^9 Hz. Given that the typical raw event size is about 1 MB, it is not possible to record all proton-proton collisions. On the other hand, the vast majority of interactions are soft collisions, which are not interesting for the search-oriented physics program CMS intends to pursue. Therefore the aim of the trigger system is that to lower the rate of acquired events to manageable levels ($\sim$100 Hz), while still retaining most of the potentially useful events.

This is achieved through a two-tier system: a Level-1 Trigger (L1) and a High-Level Trigger (HLT). The L1 system is made of a series of custom-designed, largely programmable hardware processors, whereas the HLT is a software system implemented in a computer farm made of about one thousand commercial processors. The design goal of the trigger system as a whole is that to have a reduction rate capability of 10^7.

2.2.6.1 Level-1 Trigger

The Level-1 trigger [12] reduces the rate of selected events down to 50–100 kHz. The full data are stored in pipelines of processing elements, while waiting for the trigger decision. The L1 decision whether taking or discarding data from a particular bunch crossing has to be taken in 3.2 μs; if the L1 accepts the event, the data are moved to be processed by the HLT.

To deal with the high bunch crossing rate, the L1 trigger has to take a decision in a time too short to read data from the whole detector, therefore it employs the calorimetric and muon information only, since the tracker algorithms are too slow for this purpose. The L1 trigger is organized into a Calorimeter Trigger and a Muon Trigger, whose informations are transferred to the Global Trigger which takes the final accept-reject decision.

The Calorimeter Trigger is based on trigger towers, 5×5 matrices of ECAL crystals, which match the granularity of HCAL cells. The trigger towers are grouped in 4×4 squares. The Calorimeter Trigger identifies the best four candidates of each of the following classes: electrons and photons, central jets, forward jets and τ-jets (identified from the shape of the deposited energy). The information of these objects is passed to the Global Trigger, together with the measured calorimetric missing transverse energy. The Muon Trigger is ran separately for each muon detector. The information is then merged and the best four muon candidates are transferred to the Global Trigger.

The Global Trigger takes the accept-reject decision exploiting both the characteristic of the single objects and of combinations of them.

2.2.6.2 High-Level Trigger

The High-Level Trigger [13] reduces the output rate to about 100 Hz. It is a highly-customizable software system, in which flexibility is maximized because there is complete freedom in deciding which data to access, as well as the sophistication of the adopted algorithms. The HLT software is organized in a set of algorithms (known as HLT 'paths') which are designed to select specific event topologies.

Various strategies are employed at HLT, some of which (the ones relevant for this analysis) will be shown in Sects. 2.3 and 2.4. The guiding principles are: regional reconstruction, and fast event veto. Regional reconstruction tries to avoid the complete event reconstruction, which would take time, but rather focuses on the detector regions close to where the L1 trigger has found interesting activity. Fast event veto means that uninteresting events are discarded as soon as possible, therefore freeing the processing power for the next events in line. This has led to the development of three virtual trigger levels: the first level accesses only the muon and calorimetric data, the second level adds the data of the pixel seeds, the final step reads the full event information.

2.2.7 CMS Software Components

The goals of the CMS software are to process end select events inside the HLT farm, to deliver the processed results to the experimenters within the CMS collaboration and to provide tools for them to analyze the processed information and produce physics results. The overall collection of software, now referred to as `CMSSW`, is built around a Framework, an Event Data Model, and Services needed by the simulation. The physics and utility modules are written by detector groups. The modules can be plugged into the application framework at run time, independently of the computing environment. The software should be developed keeping in mind not only performance but also modularity, flexibility, maintainability, quality assurance and documentation. CMS has adopted an object-oriented development methodology, based primarily on the `C++` programming language.

The primary goal of the CMS Framework and Event Data Model (EDM) is to facilitate the development and deployment of reconstruction and analysis software. The EDM is centered around the Event class, which holds all data that was taken during a triggered physics event as well as all data derived from the data taking (e.g. calibration and alignment constants).

The detailed CMS detector and physics simulation is currently based on the `GEANT 4` [14] simulation toolkit and the CMS object-oriented framework and event model. `GEANT 4` provides a rich set of physics processes describing electromagnetic and hadronic interactions in detail. It also provides tools for modeling the full

CMS detector and geometry and the interfaces required for retrieving information from particle tracking through these detectors and the magnetic field. The validation of GEANT 4 in the context of CMS is described in detail in [15]. The CMS GEANT 4-based simulation program uses the standard CMS software framework and utilities, as used by the reconstruction programs.

The simulation is implemented for all CMS subdetectors in both the central and forward region, including the field map of the 3.8 T solenoid. In addition, several test-beam prototypes and layouts have been simulated. The full simulation program implements the sensitive detector behavior, track selection mechanism, hit collection and digitization (i.e. detector electronic response). The detailed simulation workflow is as follows:

- a physics group configures an appropriate Monte Carlo event generator (several are used) to produce the data samples of interest;
- the production team/system runs the generator software to produce generator event data files;
- the physics group validates the generator data samples and selects a configuration for the GEANT-based simulation of CMS, with generator events as input, to produce (using the standard CMS framework) persistent hits in the detectors;
- the physics group validates these hit data which are then used as input to the subsequent digitization step, allowing for pile-up to be included. This step converts hits into digitizations which correspond to the output of the CMS electronics.

The digitization step, following the hit creation step, constitutes the simulation of the electronic readout used to acquire data by the detector. It starts from the hit positions and simulated energy losses in the detectors and produces an output that needs to be as close as possible to real data coming from CMS. Information from the generation stage (e.g. particle type and momentum) is preserved in the digitization step. The output of this step has the same format of real collision events, and therefore can be fed to the same reconstruction software chain.

Collision events are reconstructed and stored if they satisfy at least one of the High Level Trigger paths employed online. Depending on the type of HLT path which was fired, an event is stored in a given Primary Dataset, which will therefore collect events with similar topologies. Examples of Primary Datasets are Photon, DoubleMuon, DoubleElectron, SingleMuon.

2.3 Electron Reconstruction and Trigger

Electrons are reconstructed in the silicon tracker, where they form a track, and in the crystal ECAL, where they deposit their energy. The goal of electron reconstruction is therefore to successfully couple a track with an electromagnetic energy deposit, and efficiently identify these as an electron candidate, without allowing a large rate of fakes to be introduced by other charged particles, such as pions.

While traversing the tracker material, an electron not only ionizes the medium, as any charged particle, but may incur in a large energy loss via the radiation of a photon, a process commonly known as *bremsstrahlung*. As we have seen, the tracker material budget can be as large as 1.8 X_0, therefore this eventuality is not infrequent, and has to be accounted for. This is done by adapting both the track-finding algorithm and the calorimeter energy-clustering sequence.

Standard charged-track reconstruction is a pattern-recognition problem, in which the ensemble of hits released in the tracker have to be linked together in order to identify the sets of hits which arose from the passage of single charged particles. In CMS this is solved by the use of a Kalman Filter [16] algorithm, seeded in the pixel detector and in which the posterior on the particle's momentum is updated at each tracker layer. As this algorithm is optimized for particles which lose energy only via the ionization process, an indipendent track-finder is used for electrons, which has a similar functioning as the Kalman Filter, but also contemplates the possibility of a major, abrupt radiative energy loss: this algorithm is known as the Gaussian Sum Filter [17].

Bremsstrahlung not only affects the electron's trajectory, but also the shape of its ECAL energy deposit. Radiated photons will in fact give rise to indipendent satellite clusters, which must be collected in order to achieve a precise energy measurement. Because of the axial magnetic field, photons will mainly be radiated in the azimuthal direction. Therefore in the ECAL barrel the energy clustering algorithm proceeds as follows:

- search for single crystals which have collected an amount of energy above a certain threshold (1 GeV), and sort them in descreasing energy. These are the algorithm *seeds*;
- around each seed, open in the ϕ-direction a 5-crystal wide strip, reaching up to ± 17 crystals;
- add to the row which contains the seed crystal all 5-crystal rows which have a total energy larger than 0.1 GeV.

In the endcaps the algorithm is slightly different because of the geometry: it first organizes crystals in 5×5 matrices, and then groups those matrices which lie within an azimuthal distance of 0.3 rad.

The resulting sets of grouped crystals are called ECAL *superclusters*. Electron reconstruction is then simply a matter of linking a GSF track to an ECAL supercluster. This may be done both by seeding the algorithm in the calorimeter (optimal for energies larger than $\sim$50 GeV), or in the tracker (which recovers efficiency at low electron energies). Additional identification criteria, such as isolation, ECAL energy cluster shape, and track-cluster compatibility requirements are needed in order to minimize the infiltration of fake candidates. These requirements will be described in Sect. 4.2.2.

These sophisticated algorithms cannot be ran at trigger level, of course, for they would take too long. Electron triggers therefore proceed as follows:

- the L1 trigger unpacks the ECAL information in 5 $\times$ 5 crystal matrices (trigger towers);
- seeds are identified by trigger towers which pass a given transverse energy threshold;
- isolation requirements may be applied by looking at the energy of the neighboring ECAL trigger towers, and the HCAL cell directly behind the seed tower.

Level-1 seeds are passed to the High-Level trigger which further refines the electron identification process in three steps. The first step is to cluster the ECAL energy into a supercluster (as described above) and a transverse energy threshold is applied to the supercluster energy. The second step is to access the pixel information and seek hits compatible with the hypothesis that the supercluster belongs to an electron. If no hits are found the candidate is rejected. In the third and final step the full tracker information is exploited: tracks are used for isolation and the electron candidate track is matched in momentum and position to the ECAL supercluster. Details on the adopted trigger paths are given in Sect. 4.2.2.

2.4 Muon Reconstruction and Trigger

Muon tracks are reconstructed twice in the CMS detector: in the inner silicon tracker, and in the external muon chambers. Muon reconstruction starts in the muon spectrometer: the track segments which are formed in the drift tube and cathode strip chambers are linked together with a Kalman Filter algorithm, and a *standalone* muon track is formed. Given the large amount of material they have traversed in order to reach the spectrometer, the latter's resolution is degraded because of multiple scattering interactions which have modified the muon momentum. Therefore, for low and moderate transverse momenta the silicon tracker information, which measures the muons at their production in the presence of a strong magnetic field, is crucial in order to achieve high-resolution measurements.

Once the muon track is reconstructed in the spectometer, it is linked to its tracker track. This is done in two steps: first a subset of tracks is identified which roughly match the momentum and direction of the standalone track; then a more accurate tracker-spectrometer matching is performed, by considering a number of kinematic and angular variables. Figure 2.10 shows the expected muon resolution as a function of momentum when using the muon spectrometer only, the tracker only, or the full system. As can be seen for momenta of up to hundreds of GeV the tracker resolution is dominant.

The muon trigger has been designed to be redundant and efficient: all muon subdetectors are employed in the trigger logic. The DT and CSC Level-1 electronics process the information in each station, and identify stations in which hits are sought. A track finding algorithm then scans all hits and builds them into tracks, assigning them a transverse momentum. The four highest-p_{T} and best quality candidates from each subsystem are sent to the Global Muon Trigger (GMT).

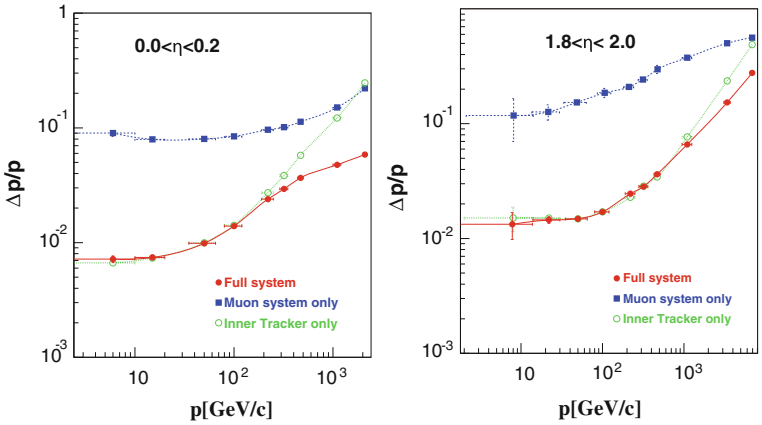

Fig. 2.10 Muon momentum resolution when using the muon spectrometers only (*squares*), the tracker only (*hollow circles*), and the full system (*solid circles*): barrel ($|\eta| < 0.2$) results are shown on the *left*, endcaps ($1.8 < |\eta| < 2.0$) on the *right*

Similarly for the RPC detectors, hits are scanned by a trigger logic and if they are aligned along a track a muon candidate is formed and assigned a transverse momentum. The candidates are ranked based on p_T and quality criteria, and the the best four in the barrel and the best four in the endcaps are kept and sent to the GMT.

The Global Muon Trigger then attempts to correlate DT and CSC candidates with the ones found in the RPC detectors. The calorimeter information is also accessed to determine the level of isolation of the muon candidate. The four best candidates are kept and passed on to the High-Level Trigger.

The muon High-Level Trigger can then impose additional selections on the candidates, such as transverse momenta and isolation requirements. This is done in two steps: the first step (Level-2) accesses the fine-grain DT and CSC information, and reconstructs the full track as seen in the muon spectrometer. The second step (Level-3) accesses the tracker information and reconstructs the complete global muon candidate.

References

1. ATLAS Collaboration.: The ATLAS experiment at the CERN large hadron collider. J. Instrum. **3**, S08003 (2008). Available from: http://stacks.iop.org/1748-0221/3/i=08/a=S08003
2. ALICE Collaboration.: The ALICE experiment at the CERN LHC. J. Instrum. **3**, S08002 (2008). Available from: http://stacks.iop.org/1748-0221/3/i=08/a=S08002
3. LHCb Collaboration.: The LHCb detector at the LHC. J. Instrum. **3**, S08005 (2008). Available from: http://stacks.iop.org/1748-0221/3/i=08/a=S08005
4. Achilli, A., Hegde, R., Godbole, R. M., Grau, A., Pancheri, G., Srivastava, Y.: Total cross-section and rapidity gap survival probability at the LHC through an eikonal with soft gluon resummation. Phys. Lett. B, **659**, 137 (2007). Comments: 15 pages, 3 figures, LaTeX

5. The CMS experiment at the CERN LHC.: J. Instrum. **3**, S08004 (2008). Available from: http://stacks.iop.org/1748-0221/3/i=08/a=S08004
6. CMS Collaboration.: The magnet project: Technical design report. CERN/LHCC 97–10, (1997)
7. CMS Collaboration.: The tracker project: Technical design Report. CERN/LHCC 98–10, (1998)
8. CMS Collaboration.: The electromagnetic calorimeter project: Technical design report. CERN/LHCC 97–33, (1997)
9. Adzic, P. et al.: Energy resolution of the barrel of the CMS Electromagnetic Calorimeter. J. Instrum. **2**, P04004 (2007). Available from: http://stacks.iop.org/1748-0221/2/i=04/a=P04004
10. CMS Collaboration.: The Hadron calorimeter project: Technical design report. CERN/LHCC 97–31, (1997)
11. CMS Collaboration.: The Muon project: Technical design report. CERN/LHCC 97–32, (1997)
12. CMS Collaboration.: The TriDAS project technical design report, vol. 1. CERN/LHCC 2000–38, (2000)
13. CMS Collaboration.: The TriDAS project technical design report, vol. 2. CERN/LHCC 2002–26, (2002)
14. Agostinelli, S. et al.: Geant 4—A Simulation Toolkit. Nucl. Inst. Meth. **A506**, 250 (2003) http://dx.doi.org/10.1016/S0168-9002(03), 01368–8
15. CMS Collaboration.: CMS physics technical design report, vol. II: Physics performance. oai:cds.cern.ch:942733. J. Phys. G. **34**, 995 (2006). Revised version submitted on 2006–09-22 17:44:47
16. Kalman, R.E.: A new approach to linear filtering and prediction problems. Trans. ASME-J. Basic Eng. **82**, 35 (1960)
17. Frühwirth, R., Speer, T.: A Gaussian-sum filter for vertex reconstruction. Nuclear instruments and methods in physics research section A: Accelerators, spectrometers, detectors and associated equipment, vol. 534, p. 217(2004). Proceedings of the IXth International Workshop on Advanced Computing and Analysis Techniques in Physics Research. Available from: http://www.sciencedirect.com/science/article/pii/S0168900204015311, http://dx.doi.org/10.1016/j.nima.2004.07.090

http://www.springer.com/978-3-319-00902-5

Search for the Standard Model Higgs Boson in the H → ZZ → l + l - qq Decay Channel at CMS

Pandolfi, F.

2013, XV, 128 p., Hardcover
ISBN: 978-3-319-00902-5